BHR Group
EXPERTS IN FLUID ENGINEERING

# Applicability of the Lattice Boltzmann Method to the simulation of pressure surges of liquid nitrogen

*Tobias Traudt, Stefan Schlechtriem*

**ABSTRACT**

Previous tests at the Fluid Transient Test Facility (FTTF) [1] revealed interesting phenomena which were unexpected like small pressure spikes in an area where only saturation pressure is expected and the almost constant velocity of vapour bubbles in cavitating flows. In order to support upcoming tests at the FTTF with liquid nitrogen (LN2), simulations were performed with a Lattice Boltzmann Method (LBM) to investigate how the LBM is suitable for this problem and to show how LN2 will be different from the tests performed with water.

Nomenclature

| | |
|---|---|
| $f$ | : distribution function |
| $t$ | : time |
| $\vec{x}$ | : coordinate |
| $\vec{\xi}$ | : particle velocity vector |
| $\tau$ | : relaxation time |
| $f^{eq}$ | : equilibrium distribution function |
| $c$ | : magnitude of velocity |
| $n,\rho$ | : density |
| $\vec{u}$ | : velocity vector |
| e | : internal energy |
| $R$ | : specific gas constant |
| $T$ | : temperature |
| $F$ | : weight |
| $s$ | : equilibrium distribution |
| $A$ | : weighting factor |
| $\Delta s$ | : lattice spacing |
| $\Delta t$ | : time step |
| $\mathcal{F}$ | : flux |
| $\Psi$ | : flux limiter |

$\Theta$ : smoothness function
$\delta_{\alpha\beta}$ : Kronecker delta function
$\mu$ : viscosity
$\kappa_e$ : heat conductivity
$\kappa$ : ratio of specific heats
$I$ : interparticle force term
$p$ : pressure

Subscripts
$k$ : index for absolute velocity
$i$ : direction index
$\alpha, \beta$ ... : vector component

## 1 INTRODUCTION

Pressure surge is of strong interest in many industrial fields, amongst which the space industry. In rocket engines and thrusters it plays a major role in the designing process of the feed system and has to be considered especially when the feed lines are primed during start-up as well as during the rapid closing of valves upon shutdown. In both cases a pressure peak will occur, leading to a pressure surge wave travelling along the pipe.
Pressure surge is a well-studied phenomenon because of its importance for the designer of fluid systems. For CFD tools it is a valuable validation experiment to check whether the code is able to correctly simulate steep pressure gradients, absolute pressure peaks and wave attenuation. When the pressure falls below the saturation pressure and hence column separation occurs, the complexity of flow simulation increases significantly because of instantaneous evaporation and condensation. In order to investigate these phenomena at pressures of up to 100 bar and Reynolds numbers of up to $10^5$ a test bench was built at the DLR Lampoldshausen. Tests were performed with water to produce a pressure surge upon valve closing.
These tests are used by industry for the validation of their numerical tools for simulating the upper stage fluid system of the upcoming Ariane 6 rocket. The Ariane 6 upper stage uses liquid oxygen (LOx) and liquid hydrogen (LH2) as fuels and of course the numerical tools need to be able to correctly handle these fuels. For this reason the FTTF will be upgraded to be able to repeat the water pressure surge experiments with LN2 and LOx. LN2 will be used first for safety reasons and after the correct operation of the FTTF with cryo-fluids has been demonstrated, the tests will be repeated with LOx. This way we will show if and how the behaviour of the cryogenic fluids is comparable to the water experiments performed at the same test bench, while creating a database of pressure surge experiments with LN2 and LOx.
In this work we will support the transition from water to cryo fluids by preliminary calculations done with a Lattice Boltzmann model which is especially suited for thermal two-phase flows. The thermal model uses the multispeed approach to enhance numerical stability [2]. The thermal model directly simulates the temperature by incorporating it into the equilibrium distribution of the distribution function. The authors who developed the thermal model proved that it is suitable for supersonic flow simulation [3]. However the Watari and Tsutahara (WT) model is for ideal gases only, so another extension of the classical LBM is needed to enable the simulation of a real gas. The chosen model is based on the WT-model and simulates a non-ideal van der Waals fluid [4].

In this paper we want to investigate how the model is able to simulate pressure surge events and we want to show how the behaviour of nitrogen is different from the behaviour of water during the pressure surge.
Three simulations have been performed with the model in order to show the above:

- **Pressure Surge in a straight conduct;** to show the overall behaviour of the LBM for this case
- **Pressure Surge with a single bubble;** to show the wave propagation over a single nitrogen vapour bubble
- **Pressure Surge with 25 bubbles;** to show the wave propagation through a duct completely obstructed by bubbles

## 2 NUMERICAL MODEL

The WT-model we use in this work is a finite difference lattice Boltzmann model (FDLBM) which is able to simulate thermal ideal gas flow by a multispeed approach. The model conserves moments up to the fourth order of flow velocity $\vec{u}$ which makes it possible to simulate compressible flow.
The extension by [4] enables the model to simulate a real gas with a van der Waals equation of state (EOS) by implementing a force term which makes it possible to simulate the interparticle forces and hence triggering phase change. The Gonella force term enhances the WT-model to the WTG-model. The mathematical foundation of both models will be presented in this section.
For validation of the interesting features for cryo-fluids, three validation cases have been simulated in [5] by the authors. Overall correct representation of incompressible single-phase flow was demonstrated by a lid driven cavity. Instantaneous evaporation was simulated by the formation of a single vapour bubble at a heated surface. And finally a Riemann shock tube configuration showed the capability of the model to handle shocks and supersonic flow [5].

### 2.1 Ideal gas multispeed model

The thermal ideal gas model is a so called multispeed model, because it uses more speeds than the classical LBM. This is done in order to increase numerical stability and to conserve moments of higher order, which makes it possible to simulate more physical phenomena like compressible flow, for example.
The Ideal gas multispeed model solves the Boltzmann equation with the Bathnagar, Kross and Grook collision term

$$\frac{\partial f}{\partial t} + \vec{\xi} \cdot \frac{\partial f}{\partial \vec{x}} = -\frac{1}{\tau}(f - f^{eq}) \tag{1}$$

where $f$ is the particle distribution function, $t$ is the time, $\vec{\xi}$ is the particle velocity vector, $\vec{x}$ the direction in Cartesian coordinates, $\tau$ the relaxation time and $f^{eq}$ the equilibrium distribution function.
The model uses a quadratic two-dimensional grid (see **Figure 1**), hence the components of the particle velocities are

$$\xi_{00} = 0, \xi_{ki} = \left[\frac{cos\,\pi(i-1)}{4}, \frac{sin\,\pi(i-1)}{4}\right] c_k, \tag{2}$$

where $i = 1, \dots, 8$ is the index for the direction and $k = 1, \dots, 4$ is the index for the set of absolute values of the velocity, $c_k$. The values for $c_k = [1.0, 1.92, 2.99, 4.49]$ were chosen in [2] to increase the stability of the model. This leads to a total number of $\xi_{00} + \xi_{ki} = 33$ velocities.
The local values for the macroscopic density $n$, the velocity $\vec{u}$ and the temperature $e$ are

$$n = \sum_{ki} f_{ki}, \tag{3}$$

$$nu_\alpha = \sum_{ki} f_{ki} \xi_{ki\alpha}, \tag{4}$$

$$n\left(e + \frac{\vec{u}^2}{2}\right) = \frac{1}{2} \sum_{ki} f_{ki} c_k^2. \tag{5}$$

$e$ is the internal energy and relates to the temperature $T$ by $e = RT$, with $R$ being the

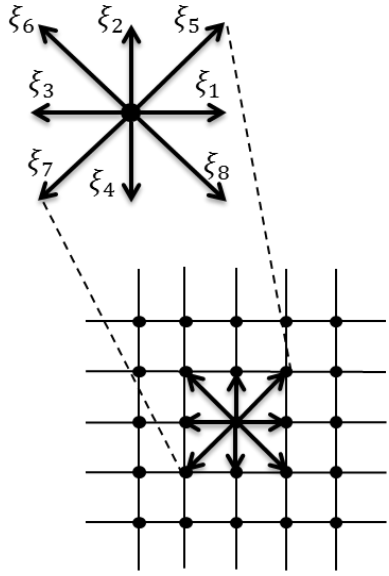


**Figure 1: Quadratic grid for discretization.**

specific gas constant.
The equilibrium distribution function has the form

$$f_{ki}^{eq} = nF_k s_{ki}, \tag{6}$$

with

$$
\begin{aligned}
s_{ki} = \left(1 - \frac{u^2}{2e} + \frac{u^4}{8e^2}\right) + \frac{1}{e}\left(1 - \frac{u^2}{2e}\right)\xi_{ki\psi}u_\psi \\
+ \frac{1}{2e^2}\left(1 - \frac{u^2}{2e}\right)\xi_{ki\psi}\xi_{ki\eta}u_\psi u_\eta \\
+ \frac{1}{6e^3}\xi_{ki\psi}\xi_{ki\eta}\xi_{ki\zeta}u_\psi u_\eta u_\zeta \\
+ \frac{1}{24e^4}\xi_{ki\psi}\xi_{ki\eta}\xi_{ki\zeta}\xi_{ki\chi}u_\psi u_\eta u_\zeta u_\chi,
\end{aligned} \tag{7}
$$

and the weights

$$
\begin{aligned}
F_k = \frac{1}{c_k^2\left(c_k^2 - c_{\{k+1\}}^2\right)\left(c_k^2 - c_{\{k+2\}}^2\right)\left(c_k^2 - c_{\{k+3\}}^2\right)} \\
\times \Big[48e^4 + 6\left(c_{\{k+1\}}^2 + c_{\{k+2\}}^2 + c_{\{k+3\}}^2\right)e^3 \\
+ \left(c_{\{k+1\}}^2 c_{\{k+2\}}^2 + c_{\{k+2\}}^2 c_{\{k+3\}}^2 + c_{\{k+3\}}^2 c_{\{k+1\}}^2\right)e^2 \\
- \frac{c_{\{k+1\}}^2 c_{\{k+2\}}^2 c_{\{k+3\}}^2}{4} e\Big] \\
F_0 = 1 - 8(F_1 + F_2 + F_3 + F_4).
\end{aligned} \tag{8}
$$

The weights $F_k$ follow the notation of [6]. Please note that summation over repeated greek indices (Einstein notation) is used in the equations above.
Since the speeds are not related to the lattice spacing, a finite difference scheme is used to discretize the model in space. We use the flux limiter scheme based on the Lax-Wendroff scheme according to [7]. Equation (1) then becomes

$$
\frac{\partial f}{\partial t} = -\frac{c_k}{A_i \Delta s}\left[F_{ki}^{n,j+1/2} - F_{ki}^{n,j-1/2}\right] - \frac{1}{\tau}\left[f_{ki}^{n,j} - f_{ki}^{eq,n,j}\right], \tag{9}
$$

where $\Delta s$ is the lattice spacing, the superscript $n$ indicates the current time step and $j$ the node relative to the current node. $A_i$ is a weighting factor. It is

$$
A_i = \begin{cases} 1, & i \in \{1,\ 3,\ 5,\ 7\} \\ \sqrt{2}, & i \in \{2,\ 4,\ 6,\ 8\} \end{cases}. \tag{10}
$$

The fluxes $\mathcal{F}_{ki}^{n,j+1/2}$ and $\mathcal{F}_{ki}^{n,j-1/2}$ are

$$
\begin{aligned}
F_{ki}^{n,j+1/2} = f_{ki}^{n,j} + \frac{1}{2}\left(1 - \frac{c_k \Delta t}{A_i \Delta s}\right)\left[f_{ki}^{n,j+1} - f_{ki}^{n,j}\right]\Psi\left(\Theta_{ki}^{n,j}\right),\ f_{ki}^{n,j} \\
= f_{ki}\left(\vec{x}_j, t\right) \\
F_{ki}^{n,j-1/2} = F_{ki}^{n,(j-1)+\frac{1}{2}}.
\end{aligned} \tag{11}
$$

where $\Psi$ is the flux limiter and $\theta$ is the smoothness function

$$
\Theta_{ki}^{n,j} = \frac{f_{ki}^{n,j} - f_{ki}^{n,j-1}}{f_{ki}^{n,j+1} - f_{ki}^{n,j}}. \tag{12}
$$

In this work we did not use the flux limiter proposed by [7] because we found the flux limiter by van-Leer to be more stable:

$$\Psi\left(\Theta_{ki}^{n,j}\right) = \begin{cases} 0, & \Theta_{ki}^{n,j} \leq 0 \\ \dfrac{2\Theta_{ki}^{n,j}}{\left(1+\Theta_{ki}^{n,j}\right)}, & 0 < \Theta_{ki}^{n,j} \end{cases} \tag{13}$$

Watari and Tsutahara showed that this discretization of Eq. (1) is equivalent to the following Navier-Stokes equations with no error after the Chapman-Enskog-expansion has been applied:

$$\begin{gathered} \frac{\partial \rho}{\partial t} + \frac{\partial}{\partial r_\alpha}(\rho u_\alpha) = 0 \\ \frac{\partial}{\partial t}(\rho u_\alpha) + \frac{\partial}{\partial r_\beta}\left(\rho u_\alpha u_\beta + P\delta_{\alpha\beta}\right) - \frac{\partial}{\partial r_\beta}\left[\mu\left(\frac{\partial u_\beta}{\partial r_\alpha} + \frac{\partial u_\alpha}{\partial r_\beta} - \frac{\partial u_\gamma}{\partial r_\gamma}\delta_{\alpha\beta}\right)\right] = 0 \\ \frac{\partial}{\partial t}\left[\rho\left(e + \frac{\vec{u}^2}{2}\right)\right] + \frac{\partial}{\partial r_\alpha}\left[\rho u_\alpha\left(e + \frac{\vec{u}^2}{2} + \frac{P}{\rho}\right)\right] \\ - \frac{\partial}{\partial r_\alpha}\left[\kappa_e \frac{\partial e}{\partial r_\alpha} + \mu u_\beta\left(\frac{\partial u_\beta}{\partial r_\alpha} + \frac{\partial u_\alpha}{\partial r_\beta} - \frac{\partial u_\gamma}{\partial r_\gamma}\delta_{\alpha\beta}\right)\right] = 0. \end{gathered} \tag{14}$$

where $P$ is the pressure, $\mu$ is the viscosity coefficient and $\kappa_e$ is the heat conductivity. They are

$$P = \rho e, \tag{15}$$

$$\mu = \rho e \tau, \tag{16}$$

$$\kappa_e = 2\rho e \tau. \tag{17}$$

### 2.2 Real gas model

The real gas model in [4] introduces a force term $I_{ki}$ which represents the interparticle attraction forces. This way it is possible to simulate phase transition as a continuous density change over the interface. In its discretized form Eq. (9) then becomes

$$\begin{aligned} f_{ki}^{n+1,j} = f_{ki}^{n,j} - \frac{c_k \Delta t}{A_i \Delta s}\left[\mathcal{F}_{ki}^{n,j+1/2} - \mathcal{F}_{ki}^{n,j-1/2}\right] \\ - \frac{\Delta t}{\tau}\left[f_{ki}^{n,j} - f_{ki}^{eq,n,j}\right] - \Delta t \cdot I_{ki}. \end{aligned} \tag{18}$$

Since the Boltzmann equation is the microscopic description of a gas, the force term leads to a real gas which obeys the van der Waals (vdW) EOS for the WTG-model.
The force term has the form

$$
\begin{aligned}
I_{ki} &= -\left[A + B_\alpha(\xi_{ki\alpha} - u_\alpha) + (C + C_q)(\xi_{ki\alpha} - u_\alpha)^2\right] f_{ki}^{eq}\,, \quad eq.\ 5 \\
A &= -2(C + C_q)e\,, \quad eq.\ 12 \\
B_\alpha &= \frac{1}{ne}\left[\partial_\alpha(p^w - ne) + \partial_\beta \Lambda_{\alpha\beta} - \partial_\alpha(\zeta \partial_\gamma u_\gamma)\right], \quad eq.\ 13 \\
C &= \frac{1}{2ne^2}\Bigg[(p^w - ne)\partial_\gamma u_\gamma + \Lambda_{\alpha\beta}\partial_\alpha u_\beta - (\zeta \partial_\gamma u_\gamma)\partial_\alpha u_\alpha + \frac{9}{8}n^2 \partial_\gamma u_\gamma \\
&\quad + K\left(-\frac{1}{2}(\partial_\gamma n)(\partial_\gamma n)(\partial_\alpha u_\alpha) - n(\partial_\gamma n)(\partial_\gamma \partial_\alpha u_\alpha)\right. \\
&\quad \left. - (\partial_\gamma n)(\partial_\gamma u_\alpha)(\partial_\alpha n)\right)\Bigg] \\
C_q &= \frac{1}{2ne^2}\partial_\alpha[2qne(\partial_\alpha e)]
\end{aligned}
\tag{19}
$$

where

$$
\Lambda_{\alpha\beta} = M\partial_\alpha n \partial_\beta n - M\left(n\nabla^2 n + \frac{|\nabla n|^2}{2}\right)\delta_{\alpha\beta} - \left[ne\partial_\gamma n \partial_\gamma\left(\frac{M}{e}\right)\right]\delta_{\alpha\beta} \tag{20}
$$

is the contribution to the pressure tensor depending on the density gradients. $M = K + He$ allows a dependence of surface tension on the temperature $e$ but in all simulations $H$ was set to 0 and $K$ was set to 0.005. This value has been chosen mainly to improve numerical stability and to counter bubble deformation by spurious currents at the interface. The latter are a common problem of multiphase codes in general, not only LBMs [8].
$\zeta$ is the bulk viscosity, $\eta$ is the shear viscosity and finally $p^w = 3ne/(3-n) - 9/8\, n^2$ is the vdW-pressure.
The WTG-model allows variation of the Prandtl number $Pr = \eta/\kappa\_e = \tau/2(\tau - q)$ through the variable $q$.

### 2.3 Boundary and initial conditions

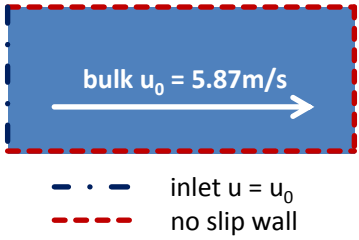


**Figure 2: Boundary conditions**

There are two types of boundary conditions (BC) which we use in this paper. A Dirichlet BC is implemented to fix values at the wall, like the velocity for example for which a no-slip wall-BC is used based on the diffuse reflection BC version 1 in [6].
The left wall and the bulk volume are set up with an initial velocity in the positive direction of $u_0 = 5.87\ m/s$, which represents a steady flow before the computation starts.

The fluid will be stopped at the right wall immediately after the simulation is started. This way a "valve" with an infinite closing speed is simulated and a pressure surge will evolve from the right wall.
The thermodynamic properties of each of the following simulations can be found in the respective chapters.

## 3 NUMERICAL SETUP AND RESULTS

Three simulations are chosen to show how nitrogen behaves in a pressure surge event. All of the 2D simulations use the same rectangular computation area with a height of 19 mm and a length of 76 mm. The height represents the same inner diameter of the pipe used in [1]. Since this work focusses on the interaction of a pressure surge with vapour bubbles formed by cavitation, the length has no impact on the wave propagation.
First a simulation of a pressure surge event with no vapour bubbles is performed. Then a single bubble is introduced in the duct to show how the incoming pressure wave is reflected at the bubble surface and how the pressure evolution in the bubble is. The last simulation presented in this work is set up with bubbles everywhere, so that the pressure wave cannot travel in the negative direction without impacting on a phase interface. I.e. there is no free path for the pressure wave in the rectangular duct.
In all simulations the bubble size is set to 26 nodes (4.9 mm) because this is a common size for the bubbles observed in the experiment.
The natural frequency of a nitrogen bubble of this size has been calculated to 62.5 kHz (according to [9]) which equals a period of 16 µs. This value is at least an order of magnitude lower than the time scale of the pressure waves simulated in this paper.
The boundary conditions are the same for all three simulations (see section 2.3).
All simulations use the real gas model, even if there is only a single phase.
The surface tension was set up in order to

### 3.1 Single phase pressure surge

The single phase simulation was set up with the properties for LN2 summarized in Table 1. The properties are for the van der Waals fluid which is simulated by the model chosen in this paper and since the vdW EOS is known to be not very accurate, they are slightly different from the real fluid properties. For this reason the third column in Table 1 shows the real fluid properties of the NIST [10] for LN2 at the temperature of 116 K.

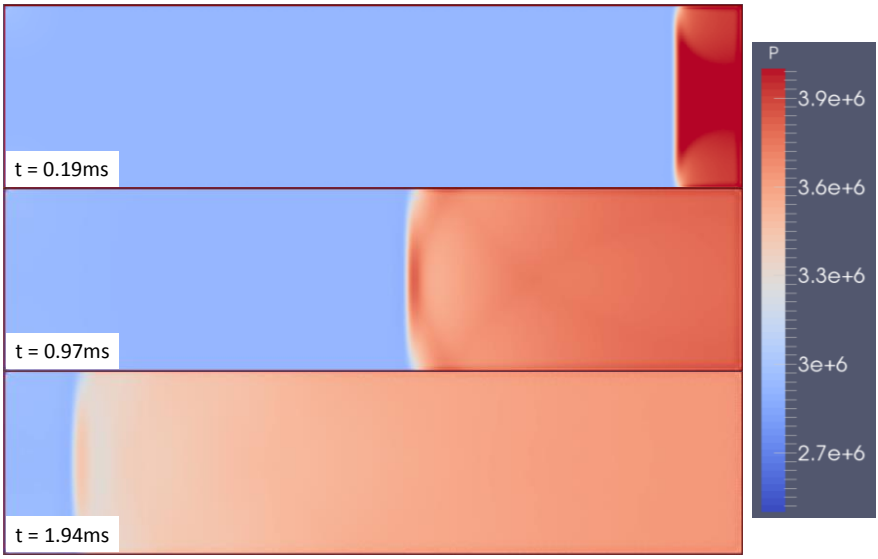


**Figure 3: Single phase pressure surge simulation**

Table 1: Fluid properties for single phase pressure surge initialization

| Property | LBM | NIST | |
|---|---|---|---|
| density $\rho$ | 519 | 586 | kg/m³ |
| temperature $T$ | 116 | 116 | K |
| pressure $p$ | 2.91 | 2.91 | MPa |
| nodes $Nx$ | 512 | | |
| nodes $Ny$ | 128 | | |

The results are shown in Figure 3. It is obvious that the LBM used in this paper has some disadvantages for simulating pressure surge. One can easily see that the dissipation of pressure is relatively high. The pressure decreases from the top picture to the bottom picture from 4.05 MPa, over 3.77 MPa to 3.63 MPa. At $t$ = 0.19 ms low pressure evolving from the wall reduces the main surge pressure. Apparently the boundary conditions are causing some of the dissipation while the numerical model itself seems to have some inherent numerical damping, too. This can also be seen in the surge pressure in the simulation, which is below the Joukowsky pressure $p_0 + \Delta p = p_0 + \rho c u_0 =$ 4.36 MPa. Here $p_0$ is the mean pressure before the pressure surge event.
Apart from that, the speed of sound is predicted well within the limits of the vdW EOS. From the distance the wave travelled and the time needed for it, a value of 473 m/s is calculated. The fluid is close to the critical point and for this reason have a relatively high sensitivity to the actual values of temperature and pressure. Depending on the pressure the speed of sound varies from 420 m/s for 2.91 MPa to 466 m/s for 4.05 MPa [10] where the latter is the pressure behind the pressure wave.

### 3.2 Single bubble pressure surge

The single bubble simulation is set up on the same rectangular grid with the same temperature, pressure and liquid density as the single phase simulation. The properties are summarized in Table 2. The properties are the saturation properties for the vdW EOS.

Table 2: fluid properties for single bubble pressure surge initialization

| | | |
|---|---|---|
| density liquid $\rho_l$ | 519 | kg/m³ |
| density vapor $\rho_v$ | 133 | kg/m³ |
| temperature $T$ | 116 | K |
| pressure $p$ | 2.91 | MPa |
| nodes $Nx$ | 512 | |
| nodes $Ny$ | 128 | |

The bubble and the liquid have the initial velocity of $u_0 = 5.87\ m/s$. The position of the bubble is at node 400 in x-direction and in the middle of the duct in y-direction. The radius of the bubble is 13 nodes (4.9 mm in diameter).
The main reason for the simulation with a single bubble is to show the pressure wave bubble interaction in a simple example. The same structures will also be visible in the simulation with more bubbles, but they will not be so easy to distinguish because they are as numerous as the number of bubbles in the simulation.
Figure 4 shows the results of the simulation. The first two pictures show a low pressure wave which originates from the bubble, as well as the pressure surge coming from the right wall. The small wave coming from the bubble is due to non-equilibrium initialization.
In the third picture at time $t$ = 0.485 ms the main pressure wave passes the bubble. One can see three effects here.

The first one is the reflection of the pressure wave at the bubble interface as a negative pressure wave.
The second effect visible is how each contact point of the main pressure wave with the interface starts a pressure wave inside the bubble, which itself travels with the lower speed of sound in the vapour in the bubble. This can also be tracked in the fourth picture. For our experiments the density ratio is 3.9 which is very close to the numerical simulation presented in [11] where a bubble of Krypton gas in air has been simulated (density ratio of 2.9). Since Krypton has a lower SOS than air the results show a comparable behaviour of the pressure distribution in the bubble. The authors validated their simulations against experimental results and achieved very good agreement [11].
The third effect visible in the third picture is the low pressure wave mentioned before which has its origin in non-equilibrium initialization. It leads to a distortion of the bubble. It is no longer round in shape, but more a square. This effect is pronounced by spurious currents at the interface. Spurious currents at phase interfaces are a known problem in numerical codes [12]. A test simulation done with a bubble without external disturbances did not show this behaviour.
Pictures 5 to 7 (0.573 ms to 0.776 ms) show that after the pressure wave inside of the bubble "collapses" or reunites at the front of the bubble, a new pressure wave is sent off from the front of the bubble which travels behind the main pressure wave of the pressure surge event. This behaviour has also been observed by [11].
One can also see, that the pressure inside the bubble reaches a maximum at $t$ = 0.776 ms. There is no bubble collapse visible. Past experiments with water showed [1] that the collapse time of a bubble is of the order of 6ms. The authors expect the same behaviour of LN2 gas bubbles as the ones observed in water. The simulation deviates here from the experimental observation. The bubble collapse is driven the so called Richtmyer-

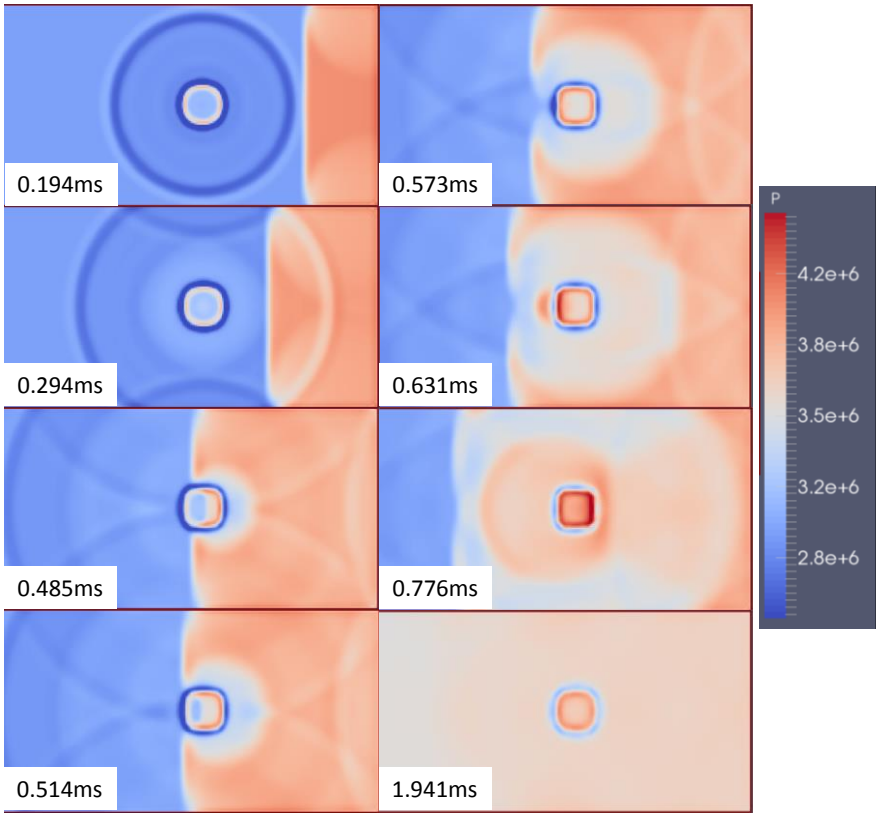


**Figure 4: Single bubble pressure surge simulation**

Meshkov instabability formed at the interface between two fluids with different densities. This instability is of small scale and could not be resolved in the numerical simulations presented in this paper. The resolution of the mesh on the initial bubble diameter is 0.19 mm. In [11] the authors were not able to reproduce the instabilities with a resolution of 0.1mm.

### 3.3 Multiple bubble pressure surge

25 circular bubbles were positioned in equal distance from each other for this simulation. This way the pressure wave cannot travel upstream without passing a liquid vapour interface. The bubbles all have a diameter of 13 nodes and a distance of 52 nodes from each other. The fluid properties are the same as for the simulation with a single bubble. The results are shown in Figure 5 and Figure 6.

Till time $t$ = 0.776 ms the behaviour of the pressure wave is comparable to the single bubble case. At time $t$ = 0.97 ms there is no pressure wave front visible anymore in between the bubbles, but the pressure inside of the bubbles is a good indication on where the pressure surge is at the moment. After 1.941 ms it is obvious that the speed of sound is lower than in the single phase case of the first simulation presented in this paper (284 m/s).

There is strong attenuation of the pressure wave. One has to keep in mind that the model in use showed numerical dissipation of pressure (see section 3.1), but nevertheless it is obvious that diffraction and reflection of the pressure wave at the phase interface also play an important role in attenuation.

As in the single bubble case bubble collapse is not visible, which is unexpected.

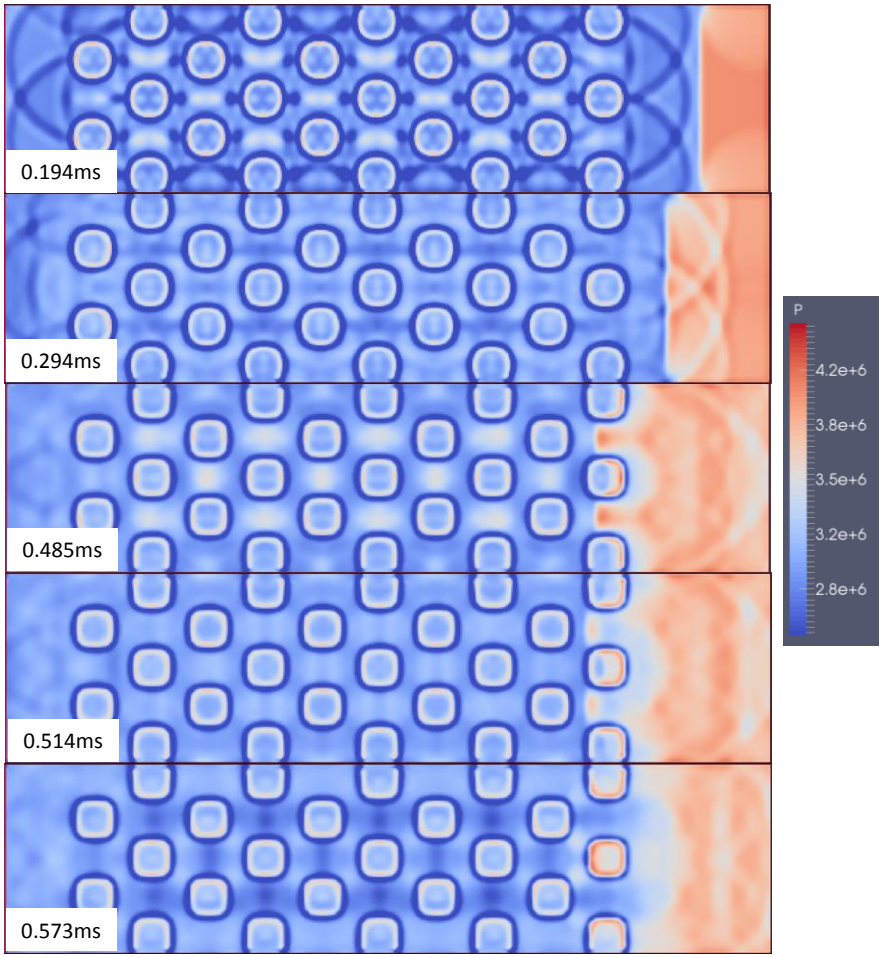


**Figure 5: 25 bubble pressure surge simulation, 0.194 ms to 0.573 ms**

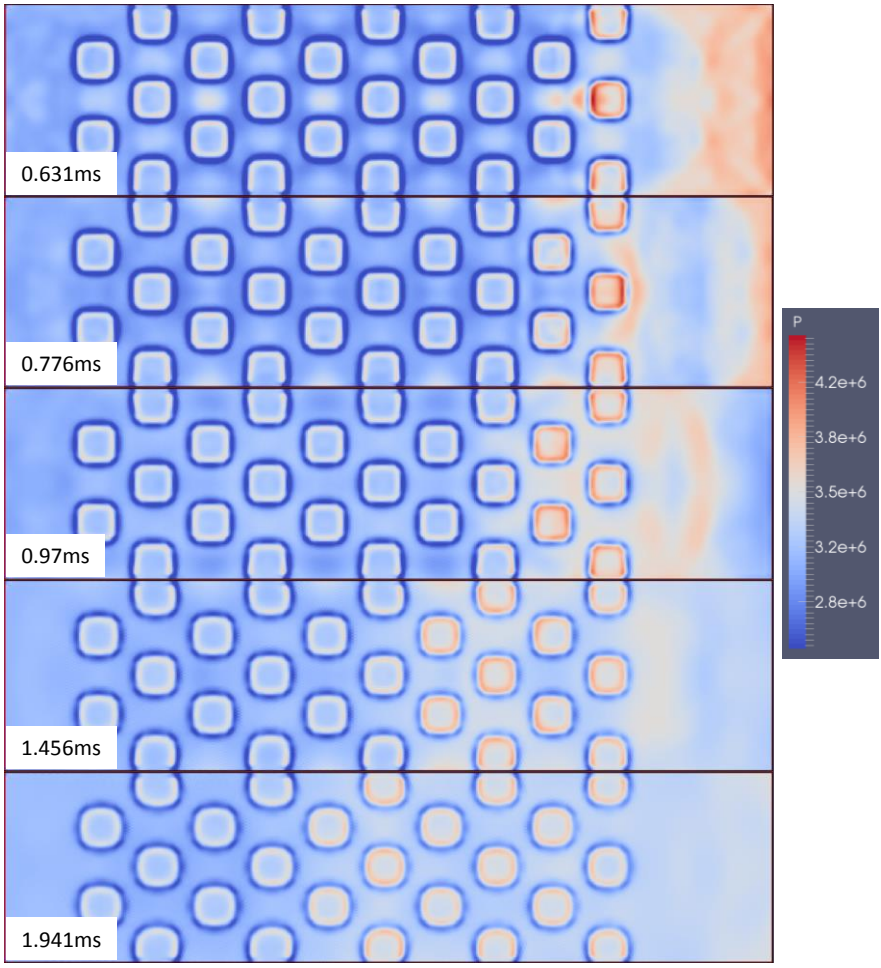


**Figure 6: 25 bubble pressure surge simulation, 0.631 ms to 1.941 ms**

## 4 CONCLUSION

Three pressure surge simulations with liquid nitrogen have been performed in order to show the applicability of the Lattice Boltzmann Method. LBM has been chosen for the simulations because it is able to simulate temperature as well as two-phase flow, by using a multi-speed finite difference approach and an additional force term.

In the simulation of a single phase liquid, the LBM performs well in predicting the speed of sound and it has overall stability, while showing minor shortcomings in the pressure attenuation and the maximum pressure peak of the pressure surge.

In two-phase flow simulations the LBM makes it easy to track pressure waves traveling over vapour-liquid interfaces. By the simulation of a single bubble in a liquid, we could show the complex interaction of the pressure wave with the bubble interface.

Finally a duct filled with bubbles was simulated. Strong pressure wave attenuation could be observed due to multiple wave scattering in the bubble cloud.

## References


[1] T. Traudt, C. Bombardieri and C. Manfletti, "High Speed Imaging of Water Hammer with Column Separation," in *Pressure Surges Conference, Dublin*, 2015.

[2] M. Watari and M. Tsutahara, "Two-dimensional thermal model of the finite-difference lattice Boltzmann method with high spatial isotropy," *Phys. Rev. E*, vol. 67, no. 3, p. 036306, 3 2003.

[3] M. Watari and M. Tsutahara, "Supersonic flow simulations by a three-dimensional multispeed thermal model of the finite difference lattice Boltzmann method," *Physica A: Statistical Mechanics and its Applications*, vol. 364, pp. 129-144, 2006.

[4] G. Gonnella, A. Lamura and V. Sofonea, "Lattice Boltzmann simulation of thermal nonideal fluids," *Phys. Rev. E*, vol. 76, no. 3, p. 036703, 9 2007.

[5] T. Traudt and S. Schlechtriem, "Validation of a Lattice Boltzmann Model for transient cryogenic two phase flow (accepted for publication in Transactions of JSASS, Aerospace Technology Japan)," 2018.

[6] V. Sofonea, "Implementation of diffuse reflection boundary conditions in a thermal lattice Boltzmann model with flux limiters," *Journal of Computational Physics*, vol. 228, pp. 6107-6118, 2009.

[7] A. Cristea, G. Gonnella, A. Lamura and V. Sofonea, "Finite-difference lattice Boltzmann model for liquid–vapor systems," *Mathematics and Computers in Simulation*, vol. 72, pp. 113-116, 2006.

[8] T. J. Chung, Computational Fluid Dynamics, Cambridge University Press, 2002.

[9] T. G. Leighton, in *The Acoustic Bubble*, Academic Press, 1994.

[10] National Institute of Standards and Technology, "Thermophysical Properties of Fluid Systems," https://webbook.nist.gov/chemistry/fluid/, 2018.

[11] J. Giordano and Y. Burtschell, "Richtmyer-Meshkov instability induced by shock-bubble interaction: Numerical and analytical studies with experimental validation," *Physics of Fluids*, vol. 18, p. 036102, 2006.

[12] P. Yuan and L. Schäfer, "Equations of state in a lattice Boltzmann model," *Physics of Fluids*, vol. 18, pp. 1-11, 2006.